Spectroelectrochemistry at free-standing carbon nanotubes electrodes.

D. Ibañez,[a,1], *J. Garoz-Ruiz*[a,1], *D. Plana*[b,c,1], *A. Heras*[a,1], *D. J. Fermín*[b,1], *A. Colina*[a,1,*]

a. *Department of Chemistry, Universidad de Burgos, Pza. Misael Bañuelos s/n, E-09001 Burgos, Spain.*

b. *School of Chemistry, University of Bristol, Cantocks Close, Bristol BS8 1TS, U.K.*

c. *Lennard-Jones Laboratories, School of Physical and Geographical Sciences, Keele University, Keele ST5 5BG, U.K.*

*Corresponding author: Tel: +34-947258817, Fax: +34-947258831. E-mail: acolina@ubu.es (Alvaro Colina).

Abstract.

A versatile and low-cost methodology for fabricating free-standing carbon nanotubes (CNT) electrodes for electrochemical and spectroelectrochemical applications is described. The uniformity, flexibility and resistance to bending of these films make them one of the most interesting membranes in a wide range of applications. CNT electrodes were characterized by Raman spectroscopy and scanning electron microscopy and their electrochemical performance was assessed employing various redox species such as ferrocenemethanol, hexacyanoferrate (II) and dopamine. Free-standing single-walled CNT electrodes exhibit good conductivity and transparency to UV-Vis radiation, making them suitable as optically transparent electrodes. This is exemplified by monitoring, using UV-Vis absorption spectroelectrochemistry, the electrodeposition of gold nanoparticles (AuNPs) on one face of the free-standing CNT electrodes, while the other face remained unmodified.

1. Introduction.

Carbon nanotubes (CNTs) are one of the most exciting and versatile materials for electrochemical purposes, exhibiting exceptional mechanic, electric, electronic and thermal properties [1–8]. CNTs can be produced using different methods, such as discharge methods, laser ablation, pyrolysis, sonochemical/hydrothermal, high-pressure carbon monoxide conversion (HiPCO) or chemical vapour deposition (CVD), leading to a variety of final properties (orientation, alignment, nanotube length, diameter, purity and density) [9,10].

CNTs have been widely used as electrodes because they show important advantages with respect to other classic electrode materials [11–14]. In particular, free-standing CNT electrodes represent an innovative factor for very attractive applications, such as

electrochemical sensors [15,16], laser absorber [16], gas flowmeter [16], gas heater [16], supercapacitors [17], in thermoacoustic applications [18] and in batteries [19,20]. Different methods have been developed for the fabrication of free-standing CNT films, the most important routes being CVD [16,21,22] and vacuum-filtration [23,24], although others such as the solvent evaporation method [25] have also been used.

In this work we present a new and easy methodology for the fabrication of free-standing single-walled carbon nanotubes (SWCNT) electrodes. The main advantages of this new method are that it is easy, quick, cheap and reproducible. Moreover, neither surfactants to disperse SWCNTs, nor complex instrumentation are required, and it can be used with all kinds of CNTs, including commercial ones. The resulting electrodes have been characterized by both Raman spectroscopy and scanning electron microscopy (SEM), providing not only structural and vibrational information of CNTs, but also information about the distribution of the nanotubes in the film. The validation of these substrates as electrodes has been tested by cyclic voltammetry with different redox couples, such as ferrocenemethanol (FcMeOH) and potassium hexacyanoferrate (II) ($K_4[Fe(CN)_6]$), chemicals that show a well-defined reversible electrochemical processes. Furthermore, the oxidation of dopamine was also studied in order to demonstrate the usefulness of these free-standing SWCNT electrodes in the study of species of interest in biochemistry.

Janus materials can be fabricated with one hydrophilic and one hydrophobic face, with an area positively charged and another negatively charged, or with different optical, magnetic or catalytic properties in each of their faces [26–29]. In fact, these structures could consist of two different organic polymeric materials, two inorganic materials, or one organic and one inorganic material [30,31]. This variety of combinations enables the application of these materials in multitude fields, such as in

the upgrade of new and more powerful sensors, in electronics, catalysis or in the development of new medical devices to facilitate the control of drug delivery [30–32]. Here, we propose the independent functionalization of one face of free-standing SWCNT film electrode. The main advantage of this procedure is that it allows the design of Janus materials with specific characteristics and very different surface chemistry properties on each face of the free-standing SWCNT film.

As proof of concept, we have selectively modified one of the faces with gold nanoparticles (AuNPs), leaving the other face unmodified. There is a substantial literature on metal NPs, specially on their synthesis, which can be accomplished using different methods such as chemical reduction [33], seed-mediated [34], photochemical [35], electrochemical [36], sonochemical [37], lithography [38], galvanic replacement [39], thermal evaporation [40], radiolysis [41], sol-gel [42], laser ablation [43] or CVD [44]. All these methods could be useful to selectively modify the electrode in one of the faces, but as our film can be used as an electrode, electrodeposition of metal NPs can be performed in a single face due to the high hydrophobicity of the SWCNT network.

It is noteworthy that our free-standing SWCNT electrodes exhibit a good transparency to UV-Vis radiation and can be used as optically transparent electrodes for UV-Vis absorption spectroelectrochemistry. This technique facilitates the study of different processes that take place on the electrode surface, being necessary both, a good transparency and a good conductivity, to get appropriate spectral and electrochemical signals. Therefore, UV-Vis absorptometric spectroelectrochemistry experiments were performed to follow the electrochemical modification of one face of the free-standing SWCNT electrode with AuNPs, demonstrating both that modification of one face is possible and that good quality UV-Vis spectra can be recorded simultaneously to the electrochemical signal.

2. Material and methods.

2.1. Reagents.

SWCNT (Sigma-Aldrich) dispersion was prepared using 1,2-dichloroethane (DCE, Acros Organics) as solvent. Nitrocellulose filters with pore size of 0.45 μm (HAWP01300, Millipore Omnipore), acetone (VWR), poly(ethylene terephthalate) (PET, 175 mm thick, HiFi Industrial Film), conductive silver paint (Electrolube) for ohmic contacts, and epoxy protective overcoat (242-SB, ESL Europe) as insulating paint were used to produce the free-standing SWCNT electrodes.

All reagents employed were of analytical grade or higher. Ferrocenemethanol, (FcMeOH, Sigma-Aldrich), potassium hexacyanoferrate (II) ($K_4[Fe(CN)_6]\cdot 3H_2O$, Merck), potassium hexacyanoferrate (III) ($K_3[Fe(CN)_6]$, Merck), potassium nitrate (KNO_3, Merck), potassium chloride, (KCl, Acros Organics), lithium chloride (LiCl, Merck), dopamine, (DA, Acros Organics), perchloric acid ($HClO_4$, 60%, Panreac) and hydrogen tetrachloroaurate (III) trihydrate ($HAuCl_4\cdot 3H_2O$, Acros Organics) were used as received. Aqueous solutions were prepared using high-quality water (resistivity of 18.2 MΩ·cm, MilliQ gradient A10 system, Millipore).

2.2. Instrumentation.

SWCNT solutions were dispersed using a CY-500 tip-sonicator (Optic ivymen System). For safety considerations, all handling and processing were performed carefully, particularly when DCE was used.

All electrochemical measurements were carried out at room temperature using a potentiostat/galvanostat AUTOLAB PGSTAT 20 electrochemical system. A free-

standing SWCNT film was used as working electrode, a Pt wire as auxiliary electrode and a homemade Ag/AgCl/KCl (3 M) as reference electrode.

Raman spectra were obtained using a Confocal Raman Voyage (BWTEK). A 20× objective was used, with an excitation line at 532 nm and a power of 5 mW. Raman spectra were collected by a CCD array, with a spectral resolution of 3.8 cm^{-1}.

Scanning electron microscopy (SEM) was performed using a JEOL field emission gun SEM 6330 and a Philips XL 30 S FEG microscope.

Atomic-force microscopy (AFM) measurements were carried out using a Alpha300R - Alpha300A AFM WITec.

UV−Vis absorption spectroelectrochemistry measurements in normal transmission configuration were performed using a QE65000 spectrometer (Ocean Optics) synchronized with the potentiostat. The light beam, supplied by a light source (AvaLight-DH-S-BAL, Avantes), was conducted to the spectroelectrochemical cell by a 230 μm optical fiber (Ocean Optics) and collected from the spectroelectrochemical cell and lead it to the spectrometer by a 200 μm optical fiber probe (Avantes).

Fig. S1 in Supporting Information illustrates the 3-component custom made spectroelectrochemical cell, fabricated in poly(methyl methacrylate) (PMMA) using a high precision CO_2 laser cutting machine (Laser Series Equipment, PC 60/40KKII). This type of cell design is well suited for highly sensitive dynamic spectroelectrochemical analysis of thin films in transmission mode [45]. The bottom compartment of the cell has a cylindrical hole in the center to place a collimating lens for illuminating the interface via an optical fiber probe. The upper piece has a rectangular space that allows us to fix the free-standing electrode and to fill the cell with a drop of the solution. This piece is also used to place the reference and counter

electrodes, and to fix the optical fiber probe that collects the light transmitted by the free-standing SWCNT electrode and is conducted to the spectrometer.

2.3. Preparation of free-standing SWCNT electrodes.

The methodology for preparing high quality free-standing SWCNT thin films is illustrated in Fig. S2 in Supporting Information. This methodology builds upon our recent studies for preparing SWCNT electrodes supported on substrates such as quartz, PET, PMMA, ITO and Al obtained by vacuum filtration [45,46]. Our new approach involves seven steps for the fabrication of free-standing SWCNT electrodes. However, the preparation of SWCNT films requires only four steps and can be completed in less than 20 min, being the rate-limiting step the complete removal of the nitrocellulose filter (15 min). Step 1 is the preparation of a stock dispersion of CNTs, 0.5 mg of SWCNTs in 100 mL of DCE. The homogenization of this suspension is a fundamental step because if the SWCNTs are not completely dispersed inhomogeneous films will be obtained. Homogeneous dispersions are achieved using a tip-sonicator, applying a power of 250 W for 10 min and reducing the power to 100 W for another 5 min. No surfactant addition or functionalization of the SWCNTs are needed to obtain a good dispersion, that is to say, SWCNTs are not modified prior to the fabrication of the free-standing electrodes.

Once a good dispersion is obtained, a known volume of the SWCNT dispersion is filtered under vacuum using a nitrocellulose filter (step 2). The filter with the SWCNT film is placed under a clean PET sheet with a hole (step 3). Different diameters from 1 to 3 mm have been tested. Gentle pressure around the edges of the filter is applied to improve adhesion of the SWCNT film. PET sheets are carefully cleaned with deionized water and dried, prior to the transfer step. The nitrocellulose filter is completely and

carefully dissolved by slow addition of acetone (step 4). Then, the SWCNT film is thoroughly rinsed with acetone for 15 min.

The SWCNT film is then dried at room temperature (step 5), before an ohmic contact is made using a conductive silver paint (step 6). The silver paint is dried in an oven at 75 °C for 45 min, and allowed to cool before coating the contact using insulating paint (step 7). The electrode is placed in an oven at 75 °C for 120 min to dry the insulating paint.

The main advantages of this method can be summarized as an easy formation and transference of the free-standing SWCNT films by adding acetone to the nitrocellulose filter, the quickness of the procedure, the leaving out of special instrumentation and the comsumption of low amounts of reagents and, specially, the good reproducibility obtained with different kinds of SWCNTs.

3. Results and Discussion.

3.1. Characterization of the free-standing SWCNT electrodes.

Characterization of these electrodes was performed by different techniques, including SEM and Raman spectroscopy. Free-standing SWCNT electrodes of several diameters (1, 2 and 3 mm) were fabricated. Fig. 1 displays the SEM image of a 2 mm free-standing SWCNT film. As can be observed, the film is completely uniform, the morphology does not show differences and only small folds are present in the film. Moreover, Fig. 1 illustrates the evenness of the film even in the limit of the PET sheet. Another important property of these electrodes is the flexibility. Even when the PET sheet is completely bent in any direction (Fig. 2), the free-standing SWCNT film remains intact, not showing any cracks, i.e, the film shows exceptional flexibility properties.

Spectroscopic characterization was performed by Raman spectroscopy, due to the valuable information on the vibrational properties of nanotubes that this technique provides [47–51]. It allows us to verify that the integrity of the SWCNTs is not affected during the electrode fabrication. Free-standing SWCNT electrodes were characterized focusing the laser on the SWCNT area without physical support. A characteristic Raman spectrum of the SWCNTs (Fig. 3, red line) shows mainly four bands: the radial breathing mode (RBM), the disorder induced mode (D), the tangential displacement mode (G) and the high frequency two phonon mode (G') [47–52]. These bands are completely similar before and after preparation of the film.

The RBM band appears around 150-250 cm^{-1} in the Raman spectrum and provides suitable information about the diameter of the SWCNTs. There are as many different SWCNT diameters as RBM bands are distinguished in the spectrum. The diameter value is calculated using a relationship with several semiempirical parameters (eq. S1 in Supporting Information) [49]. SWCNTs used in this work show two RBM bands located at 156 cm^{-1} and 174 cm^{-1}, that correspond to diameters of 1.56 nm and 1.38 nm for the different SWCNTs in the film. The most intense band, the G-band, is located at 1550-1600 cm^{-1} and it is related to the tangential vibration modes of the SWCNTs [49]. This band involves several peaks related to two effects: (1) the symmetry effect linked to the SWCNT curvature, and (2) the phonon wave vector confinement along the circumferential direction. This Raman band has two components, one centered at about 1570 cm^{-1} (G^-) and other around 1590 cm^{-1} (G^+). The G^- component is associated with the vibration of carbon atoms along the circumferential direction of the SWCNTs, being highly sensitive to the metallic or semi-metallic character of the film. Its frequency depends on the diameter and the metallic or semi-metallic properties, but not on the chiral angle. The G^+ mode is associated with the vibration of the carbon atoms along the

nanotube axis and its frequency is sensitive to the charge transfer from dopant additions (up-shifts for acceptors and down-shifts for donors), but it is independent of the chiral angle and the diameter. The small D-band, centred around 1250-1450 cm^{-1}, corresponds to the presence of defects, such as substitutional heteroatoms, vacancies, grain boundaries, and finite size effects, all of which lower the crystalline symmetry of the quasi-infinite lattice. The G'-band, centred at 2500-2800 cm^{-1} is an overtone of the D-band and both, the D and G' bands, are the result of second-order Raman scattering processes. However, the G'-band appears even in crystalline graphite where the D-band is absent, so the G'-band is an intrinsic characteristic of the graphene lattice.

The Raman spectrum of the nitrocellulose filter is also shown in Fig. 3 (blue line). The bands observed in the spectrum are: 2972 and 2922 cm^{-1} (CH_2 stretching), 1650 cm^{-1} (N–O asymmetric stretching), 1455 cm^{-1} (CH_2 scissoring), 1427 cm^{-1} (C–OH scissoring), 1383 cm^{-1} (C–H scissoring), 1313 cm^{-1} (CH_2 wagging), 1279 cm^{-1} (N–O symmetric stretching), 1205, 1162, 1119, 1070, 1024 and 1002 cm^{-1} (C–O stretching), 946 and 915 cm^{-1} (C–H scissoring), 836 cm^{-1} (N–O stretching), 746 cm^{-1} (NO_2 wagging), 685 cm^{-1} (pyranose), 639 and 625 cm^{-1} (NO_2 rocking) and 541 cm^{-1} (pyranose) [53,54]. The nitrocellulose Raman bands are absent in the spectrum corresponding to the SWCNT free-standing film, with only bands related to SWCNTs appearing in the Raman spectrum; these results confirm that the nitrocellulose filter is essentially removed upon addition of acetone.

3.2. Electrochemical assessment of the free-standing SWCNT electrodes.

Fig. 4 shows the cyclic voltammograms of 5×10^{-4} M FcMeOH in 0.1 M KCl, scanning the potential between -0.10 V and +0.60 V, at different scan rates. A linear relationship between current density peaks (j_p) and the square root of the potential scan

rates ($v^{1/2}$), shown in the insets of Fig. 4, confirms the reversible (*i.e.* diffusion controlled) behaviour of this redox couple at the SWCNT film [45,55]. The same experiment was performed using sides A (Fig. 4.a) and B (Fig. 4.b) as working electrode, showing very similar responses. These two sides or faces differ in the active area in electrochemical measurements, being higher in side A than in side B (Fig. 5.a).

Comparison between the current obtained when side A or side B are used in electrochemical experiments is very representative of the working electrode area. Fig. 5.b displays the cyclic voltammograms obtained at 0.01 V s^{-1} depending on the side used. The intensity of the anodic peak when side A (blue line) is used as working electrode, $I_{p\ (side\ A)}$=1.90 × 10^{-5} A, is higher than when side B (red line) is selected, $I_{p\ (side\ B)}$=3.49 × 10^{-6} A, due to the different electrode areas. The geometrical areas (A_A and A_B) can be calculated using the Randles–Sevcik equation (eq. S2 in Supporting Information), obtaining 0.550 ± 0.006 cm^2 and 0.100 ± 0.004 cm^2 for the working electrode area of side A and B, respectively. These values perfectly agree with the different geometrical area (Fig. 5.a) delimited in the two sides of the electrode. The free-standing film has a geometrical area of 0.090 ± 0.006 cm^2 in contact with the solution in side B, delimited by the size of the hole, whereas side A has a higher geometrical area, 0.550 ± 0.006 cm^2, delimited by the insulating paint used to isolate the ohmic contact. According to these results, the ratio between the areas calculated from the peak current values of the voltammograms registered of the two sides is A_A/A_B = 5.50, in good agreement with the expected value from geometrical areas, 6.11. In addition, these experiments demonstrate that due to the high hydrophobicity of the SWCNTs, these electrodes are not permeable to aqueous solutions. Electrolyte penetration would lead to a high double layer charging current. The significantly larger

faradaic response with respect to the background capacitive current confirms the low porosity of the films [56].

Fig. S3 in Supporting Information shows the cyclic voltammograms of 5×10^{-5} M $K_4[Fe(CN)_6]$ in 0.1 M LiCl, scanning the potential between +0.10 V to +0.80 V, at different scan rates, using side B as working electrode, i.e only the free-standing face. Again, the electrochemical response obtained matches the expected response, $K_4[Fe(CN)_6]$ is oxidized to $K_3[Fe(CN)_6]$ during the anodic scan and it is reduced to recover the initial $K_4[Fe(CN)_6]$ in a reversible process [57,58]. Using the Randles–Sevcik equation and the geometrical area previously calculated (0.100±0.004 cm^2), the diffusion coefficient of $K_4[Fe(CN)_6]$ was assessed, obtaining a value of $D=6.46 \times 10^{-6}$ $cm^2\ s^{-1}$. This diffusion coefficient agrees with the literature value of $D=6.50 \times 10^{-6}$ $cm^2\ s^{-1}$ [59]. The results obtained using FcMeOH and $K_4[Fe(CN)_6]$ as reference systems demonstrate the validity of these electrodes.

Furthermore, dopamine oxidation was studied to demonstrate the utility of the free-standing SWCNT electrodes for the study of biological relevant systems. Fig. S4 in the Supporting Information shows the linear voltammetry of 5×10^{-5} M dopamine in 1.1 M $HClO_4$, scanning the potential from +0.40 V to +0.80 V, at different scan rates, using side B as working electrode. The anodic peak, observed at +0.65 V, is related to the oxidation of dopamine to dopaminequinone and is in agreement with previous works [60,61], demonstrating the utility of our electrodes in the study of relevant species to biological applications.

3.3. Electrodeposition of Au-Nanoparticles at free-standing SWCNT electrodes.

Optical transparency of the film was evaluated by measuring the transmittance at 550 nm. According to previous works [46] the transparency of these electrodes depends on the volume of the SWCNT dispersion filtered. Transmittance values at 550 nm of different free-standing films are: 29 ± 2 % with those prepared with 2 mL of the SWCNT dispersion, 18 ± 2 % for electrodes obtained filtering 3 mL, and 7 ± 2 % for electrodes fabricated with 4 mL of the SWCNT dispersion. These values demonstrate that free-standing films are useful in the study by UV-Vis spectroelectrochemistry of different processes that take place in both side A and side B of the membrane. However, the physical stability of the film is linked to the amount of SWCNTs filtered, with more stable films obtained with higher volumes; i.e. films prepared by filtering 4 mL are more stable than those prepared with 2 mL, which are more fragile. Therefore, transparency and physical stability are inversely proportional factors. Analyzing transparency and stability properties, free-standing SWCNT electrodes prepared with 3 mL of the SWCNT dispersion exhibit the optimal properties. Thickness of the 3 mL film was determined by AFM, obtaining a value of 570 ± 30 nm. The long-term stability of the 3 mL free-standing SWCNT electrode was evaluated performing cyclic voltammetry in a 5×10^{-3} M FcMeOH in 0.1 M KCl, with the electrode being in continuous contact with the FcMeOH aqueous solution. The evolution of the current of the anodic peak with time is summarized in Table S1 in Supporting Information. The anodic peak shows similar values for 20 min, with a relative variation of only 1.52 % being observed. After 20 min, the current changes progressively, 5.27 % at 30 min, 9.58 % at 45 min and 11.81 % after 60 min. These values depend on the type of SWCNT

used for the preparation of the films. Particularly, the evolution of the peak current with time depends strongly on the type and number of defects.

One of the most important aspects of the free-standing electrodes is related to the capability of these CNT films to be modified. The functionalization of side B was carried out by the electrodeposition of AuNPs. Fig. 6.a displays the chronoamperogram registered for the AuNPs electrodeposition on side B of a free-standing SWCNT electrode, at -1.50 V for 10 s, in a 2.5×10^{-3} M $HAuCl_4$ aqueous solution, using 0.1 M KCl as supporting electrolyte. UV-Vis spectra (Fig. 6.b), show an absorbance band centred around 570 nm that emerges and increases during the electrodeposition process. This absorption band corresponds to the plasmon band of AuNPs and, thus, demonstrates the electrodeposition of AuNPs on the electrode. The position and shape of the plasmon band depend on the size [62], shape [63] and density [64] of AuNPs. In this case, the absorbance band is symmetrical and centred at a somewhat higher wavelength than expected, indicating that spherical AuNPs are generated.

SEM images of the film before and after AuNPs electrodeposition are shown in Fig. 6.c and Fig. 6.d, respectively. The images confirm not only that the SWCNTs are randomly oriented without any specific orientation in the film, but also that spherical AuNPs are electrogenerated on the SWCNT surface. Moreover, this experiment also demonstrates that the free-standing electrodes can be used as optically transparent electrodes for UV-Vis absorption spectroelectrochemistry experiments, giving an added value to this type of electrodes. As can be seen here, one face of the free-standing SWCNT film electrode can be functionalized independently of the other, allowing the simple design of Janus materials.

4. Conclusions.

A novel fabrication process to prepare free-standing SWCNT electrodes has been developed. This method allows their rapid and facile fabrication by a simple and effective procedure. The electrodes have been characterized by Raman spectroscopy and SEM. The Raman spectrum shows four bands related to the SWCNTs (RBM, D-band, G-band and G'-band) and no nitrocellulose bands are observed, demonstrating the complete removal of the filter by adding acetone. SEM images show not only a random distribution of SWCNTs in the film but also the uniformity of the network. The good electrochemical performance of the free-standing SWCNT films has been demonstrated using different electrochemical systems, such as FcMeOH, $K_4[Fe(CN)_6]$ and dopamine. Quite importantly, the good transparency exhibited by the free-standing SWCNT electrodes allows performing UV-Vis absorption spectroelectrochemistry, facilitating the study of the electrochemical processes that take place in this type of electrodes. Finally, the nature of one side of the electrode has been independently modified with respect to the other face. The electrochemical functionalization of one face with AuNPs shows that the modification of the free-standing electrodes is not a complex process. The characteristics of this kind of electrodes offer the possibility of designing Janus films with specific properties that open new gates for future and very attractive applications.

Appendix A. Supplementary data.

Supplementary information associated with this article can be found in the online version.

Acknowledgments.

The financial support made by the Ministerio de Economía y Competitividad (CTQ2014-55583-R, CTQ2014-61914-EXP, CTQ2015-71955-REDT) and Junta de Castilla y León (BU033U16) are gratefully acknowledged. DI thanks Ministerio de Economía y Competitividad for his postdoctoral fellowship (CTQ2014-61914-EXP). Jose Manuel Díez is acknowledged for his help in the fabrication of the electrodes (contract funded by the European Social Fund and the Youth Employment Initiative). DP and DJF acknowledge the financial support by the Engineering and Physical Sciences Research Council (EPSRC grant EP/K007025/1). Electron microscopy studies were performed in the Chemistry Imaging Facility at the University of Bristol (partly funded by the EPSRC through EP/K035746/1 and EP/M028216/1). SIdI of Universidad Autónoma de Madrid and Isidoro Poveda are acknowledged for SEM images.

References.

[1] C. Nützenadel, Electrochemical Storage of Hydrogen in Nanotube Materials, Electrochem. Solid-State Lett. 2 (1999) 30–32.

[2] R.H. Baughman, A.A. Zakhidov, W.A. de Heer, Carbon nanotubes-the route toward applications, Science. 297 (2002) 787–792.

[3] E. Katz, I. Willner, Biomolecule-functionalized carbon nanotubes: applications in nanobioelectronics, ChemPhysChem. 5 (2004) 1084–1104.

[4] F. Pico, J.M. Rojo, M.L. Sanjuan, A. Anson, A.M. Benito, M.A. Callejas, W.K. Maser, M.T. Martinez, Single-Walled Carbon Nanotubes as Electrodes in Supercapacitors, J. Electrochem. Soc. 151 (2004) A831–A837.

[5] S. Ghosh, A.K. Sood, N. Kumar, Carbon nanotube flow sensors, Science. 299 (2003) 1042–1044.

[6] A. Bachtold, P. Hadley, T. Nakanishi, C. Dekker, Logic circuits with carbon nanotube transistors, Science. 294 (2001) 1317–1320.

[7] S.J. Tans, A.R.M. Verschueren, C. Dekker, Room-temperature transistor based on a single carbon nanotube, Nature. 393 (1998) 49–52.

[8] A. Star, E. Tu, J. Niemann, J.-C.P. Gabriel, C.S. Joiner, C. Valcke, Label-free detection of DNA hybridization using carbon nanotube network field-effect transistors, Proc. Natl. Acad. Sci. 103 (2006) 921–926.

[9] J. Prasek, J. Drbohlavova, J. Chomoucka, J. Hubalek, O. Jasek, V. Adam, R. Kizek, Methods for carbon nanotubes synthesis-review, J. Mater. Chem. 21 (2011) 15872–15884.

[10] A. Szabo, C. Perri, A. Csato, G. Giordano, D. Vuono, J.B. Nagy, Synthesis Methods of Carbon Nanotubes and Related Materials, Materials. 3 (2010) 3092–3140.

[11] L. Hu, G. Gruner, D. Li, R.B. Kaner, J. Cech, Patternable transparent carbon nanotube films for electrochromic devices, J. Appl. Phys. 101 (2007) 016102.

[12] R. Malavee Osuna, V. Hernandez, J.T. Lopez-Navarrete, E.I. Kauppinen, V. Ruiz, Ultrafast and High-Contrast Electrochromism on Bendable Transparent Carbon Nanotube Electrodes, J. Phys. Chem. Lett. 1 (2010) 1367–1371.

[13] P. Yañez-Sedeño, J.M. Pingarron, J. Riu, F.X. Rius, Electrochemical sensing based on carbon nanotubes, TrAC Trends Anal. Chem. 29 (2010) 939–953.

[14] M. Trojanowicz, Analytical applications of carbon nanotubes: a review, TrAC Trends Anal. Chem. 25 (2006) 480–489.

[15] F. Liu, Y. Piao, K.S. Choi, T.S. Seo, Fabrication of free-standing graphene composite films as electrochemical biosensors, Carbon. 50 (2012) 123–133.

[16] A.G. Nasibulin, A. Kaskela, K. Mustonen, A.S. Anisimov, V. Ruiz, S. Kivistö, et al., Multifunctional free-standing single-walled carbon nanotube films, ACS Nano. 5 (2011) 3214–3221.

[17] Z. Niu, W. Zhou, J. Chen, G. Feng, H. Li, W. Ma, J. Li, H. Dong, Y. Ren, D. Zhao, Compact-designed supercapacitors using free-standing single-walled carbon nanotube films, Energy Environ. Sci. 4 (2011) 1440-1446.

[18] B.J. Mason, S.-W Chang, J. Chen, S.B. Cronin, A.W. Bushmaker, Thermoacoustic transduction in individual suspended carbon nanotubes, ACS Nano, 9 (2015) 5372-5376.

[19] L. Noerochim, J.-Z. Wang, S.-L. Chou, D. Wexler, H.-K. Liu, Free-standing single-walled carbon nanotube/SnO_2 anode paper for flexible lithium-ion batteries, Carbon. 50 (2012) 1289–1297.

[20] S.Y. Chew, S.H. Ng, J. Wang, P. Novák, F. Krumeich, S.L. Chou, et al., Flexible free-standing carbon nanotube films for model lithium-ion batteries, Carbon. 47 (2009) 2976–2983.

[21] A. Moisala, A.G. Nasibulin, D.P. Brown, H. Jiang, L. Khriachtchev, E.I. Kauppinen, Single-walled carbon nanotube synthesis using ferrocene and iron pentacarbonyl in a laminar flow reactor, Chem. Eng. Sci. 61 (2006) 4393–4402.

[22] W.Z. Li, S.S. Xie, L.X. Qian, B.H. Chang, B.S. Zou, W.Y. Zhou, et al., Large-scale synthesis of aligned carbon nanotubes, Science. 274 (1996) 1701–1703.

[23] P. Aldeanueva-Potel, M.A. Correa-Duarte, R.A. Alvarez-Puebla, L.M. Liz-Marzan, Free-standing carbon nanotube films as optical accumulators for multiplex SERRS attomolar detection, ACS Appl. Mater. Interfaces. 2 (2010) 19–22.

[24] Z. Shi, X. Chen, X. Wang, T. Zhang, J. Jin, Fabrication of superstrong ultrathin free-standing single-walled carbon nanotube films via a wet process, Adv. Funct. Mater. 21 (2011) 4358–4363.

[25] H. Gu, T.M. Swager, Fabrication of free-standing, conductive, and transparent carbon nanotube films, Adv. Mater. 20 (2008) 4433–4437.

[26] X. Ji, Q. Zhang, F. Liang, Q. Chen, X. Qu, C. Zhang, Q. Wang, J. Li, X. Song, Z. Yang, Ionic liquid functionalized Janus nanosheets, Chem. Commun. 50 (2014) 5706–5709.

[27] S. Fujii, M. Kappl, H.-J. Butt, T. Sugimoto, Y. Nakamura, Soft Janus colloidal crystal film, Angew. Chemie Int. Ed. 51 (2012) 9809–9813.

[28] E. Shaviv, O. Schubert, M. Alves-Santos, G. Goldoni, R. Di Felice, F. Vallee, N. Del Fatti, U. Banin, C. Sönnichsen , Absorption Properties of Metal-Semiconductor Hybrid Nanoparticles, ACS Nano. 5 (2011) 4712–4719.

[29] L. Hong, A. Cacciuto, E. Luijten, S. Granick, Clusters of Charged Janus Spheres, Nano Lett. 6 (2006) 2510-2514.

[30] A. Walther, A.H.E. Muller, Janus Particles: Synthesis, Self-Assembly, Physical Properties, and Applications, Chem. Rev. 113 (2013) 5194-5261.

[31] X. Pang, C. Wan, M. Wang, Z. Lin, Strictly biphasic soft and hard Janus structures: synthesis, properties, and applications, Angew. Chemie Int. Ed. 53 (2014) 5524–5538.

[32] S. Chen, S.-Z. Qiao, Hierarchically porous nitrogen-doped graphene-$NiCo_2O_4$ hybrid paper as an advanced electrocatalytic water-splitting material, ACS Nano. 7 (2013) 10190–10196.

[33] M.-C. Daniel, D. Astruc, Gold Nanoparticles: Assembly, Supramolecular Chemistry, Quantum-Size-Related Properties, and Applications Toward Biology, Catalysis, and Nanotechnology, Chem. Rev. 104 (2004) 293–346.

[34] V. Sharma, K. Park, M. Srinivasarao, Colloidal dispersion of gold nanorods: Historical background, optical properties, seed-mediated synthesis, shape separation and self-assembly, Mater. Sci. Eng. R Reports. 65 (2009) 1–38.

[35] X. Huang, X. Zhou, S. Wu, Y. Wei, X. Qi, J. Zhang, F. Boey, H. Zhang, Reduced graphene oxide-templated photochemical synthesis and in situ assembly of Au nanodots to orderly patterned Au nanodot chains, Small. 6 (2010) 513–516.

[36] D. Ibañez, C. Fernandez-Blanco, A. Heras, A. Colina, Time-Resolved Study of the Surface-Enhanced Raman Scattering Effect of Silver Nanoparticles Generated in Voltammetry Experiments, J. Phys. Chem. C. 118 (2014) 23426–23433.

[37] A. Gedanken, Using sonochemistry for the fabrication of nanomaterials, Ultrason. Sonochem. 11 (2004) 47–55.

[38] C.L. Haynes, R.P. Van Duyne, Nanosphere Lithography: A Versatile Nanofabrication Tool for Studies of Size-Dependent Nanoparticle Optics, J. Phys. Chem. B. 105 (2001) 5599–5611.

[39] Y. Sun, Direct growth of dense, pristine metal nanoplates with well-controlled dimensions on semiconductor substrates, Chem. Mater. 19 (2007) 5845–5847.

[40] M. Frank, M. Baumer, From atoms to crystallites: Adsorption on oxide-supported metal particles, Phys. Chem. Chem. Phys. 2 (2000) 3723–3737.

[41] B.D. Du, D. V Phu, N.N. Duy, N.T.K. Lan, V.T.K. Lang, N.V.K. Thanh, N.T.P. Phong, N.Q. Hien, Preparation of colloidal silver nanoparticles in poly(N-vinylpyrrolidone) by γ-irradiation, J. Exp. Nanosci. 3 (2008) 207–213.

[42] R. Narayanan, M.A. El-Sayed, Catalysis with transition metal nanoparticles in colloidal solution: Nanoparticle shape dependence and stability, J. Phys. Chem. B. 109 (2005) 12663–12676.

[43] C. Domingo, V. Resta, S. Sanchez-Cortes, J. V Garcia-Ramos, J. Gonzalo, Pulsed laser deposited au nanoparticles as substrates for surface-enhanced vibrational spectroscopy, J. Phys. Chem. C. 111 (2007) 8149–8152.

[44] A.M. Boies, J.T. Roberts, S.L. Girshick, B. Zhang, T. Nakamura, A. Mochizuki, SiO_2 coating of silver nanoparticles by photoinduced chemical vapor deposition, Nanotechnology. 20 (2009) 295604.

[45] J. Garoz-Ruiz, A. Heras, S. Palmero, A. Colina, Development of a Novel Bidimensional Spectroelectrochemistry Cell Using Transfer Single-Walled Carbon Nanotubes Films as Optically Transparent Electrodes, Anal. Chem. 87 (2015) 6233–6239.

[46] J. Garoz-Ruiz, S. Palmero, D. Ibañez, A. Heras, A. Colina, Press-transfer optically transparent electrodes fabricated from commercial single-walled carbon nanotubes, Electrochem. Commun. 25 (2012) 1–4.

[47] M.S. Dresselhaus, A. Jorio, M. Hofmann, G. Dresselhaus, R. Saito, Perspectives on carbon nanotubes and graphene Raman spectroscopy, Nano Lett. 10 (2010) 751–758.

[48] P.W. Ruch, L.J. Hardwick, M. Hahn, A. Foelske, R. Kötz, A. Wokaun, Electrochemical doping of single-walled carbon nanotubes in double layer capacitors studied by in situ Raman spectroscopy, Carbon. 47 (2009) 38–52.

[49] M.S. Dresselhaus, G. Dresselhaus, R. Saito, A. Jorio, Raman spectroscopy of carbon nanotubes, Phys. Rep. 409 (2005) 47–99.

[50] L. Kavan, L. Dunsch, Spectroelectrochemistry of carbon nanostructures, ChemPhysChem. 8 (2007) 974–998.

[51] D. Ibañez, E.C. Romero, A. Heras, A. Colina, Dynamic Raman spectroelectrochemistry of single walled carbon nanotubes modified electrodes using a Langmuir-Schaefer method, Electrochim. Acta. 129 (2014) 171–176.

[52] M. Kalbac, Y.-P. Hsieh, H. Farhat, L. Kavan, M. Hofmann, J. Kong, M.S. Dresselhaus, Defects in individual semiconducting single wall carbon nanotubes: Raman spectroscopic and in situ Raman spectroelectrochemical study, Nano Lett. 10 (2010) 4619–4626.

[53] D.S. Moore, S.D. McGrane, Comparative infrared and Raman spectroscopy of energetic polymers, J. Mol. Struct. 661-662 (2003) 561–566.

[54] K. Castro, S.F.O. De Vallejuelo, I. Astondoa, F.M. Goñi, J.M. Madariaga, Analysis of confiscated fireworks using Raman spectroscopy assisted with SEM-EDS and FTIR, J. Raman Spectrosc. 42 (2011) 2000–2005.

[55] C. Cannes, F. Kanoufi, A.J. Bard, Cyclic voltammetry and scanning electrochemical microscopy of ferrocenemethanol at monolayer and bilayer-modified gold electrodes, J. Electroanal. Chem. 547 (2003) 83–91.

[56] H. Zanin, P.W. May, R.L. Harniman, T. Risbridger, E.J. Corat, D.J. Fermin, High surface area diamond-like carbon electrodes grown on vertically aligned carbon nanotubes, Carbon. 82 (2015) 288–296.

[57] C.A. Rodrigues, E. Stadler, M.C.M. Laranjeira, V. Drago, The preparation and characterization of the hexacyanides immobilized in chitosan, J. Braz. Chem. Soc. 8 (1997) 7–11.

[58] H.E.A. Ferreira, D. Daniel, M. Bertotti, E.M. Richter, A novel disposable electrochemical microcell: Construction and characterization, J. Braz. Chem. Soc. 19 (2008) 1538–1545.

[59] A. Bard, L. Faulkner, Electrochemical Methods. Fundamentals and applications, 2nd ed., New York: Wiley, 2001.

[60] N. González-Dieguez, A. Colina, J. Lopez-Palacios, A. Heras, Spectroelectrochemistry at screen-printed electrodes: Determination of dopamine, Anal. Chem. 84 (2012) 9146–9153.

[61] F. Zhang, G. Dryhurst, Oxidation Chemistry of Dopamine: Possible Insights into the Age-Dependent Loss of Dopamimergic Nigrostrital Neurons, Bioorg. Chem. 21 (1993) 392–410.

[62] C. Fernandez-Lopez, C. Mateo-Mateo, R.A. Alvarez-Puebla, J. Perez-Juste, I. Pastoriza-Santos, L.M. Liz-Marzan, Highly controlled silica coating of PEG-capped metal nanoparticles and preparation of SERS-encoded particles, Langmuir. 25 (2009) 13894–13899.

[63] C.-J. Huang, P.-H. Chiu, Y.-H. Wang, C.-F. Yang, Synthesis of the gold nanodumbbells by electrochemical method, J. Colloid Interface Sci. 303 (2006) 430–436.

[64] N.J. Halas, S. Lal, W.-S. Chang, S. Link, P. Nordlander, Plasmons in strongly coupled metallic nanostructures, Chem. Rev. 111 (2011) 3913–3961.

Figures

Figure 1

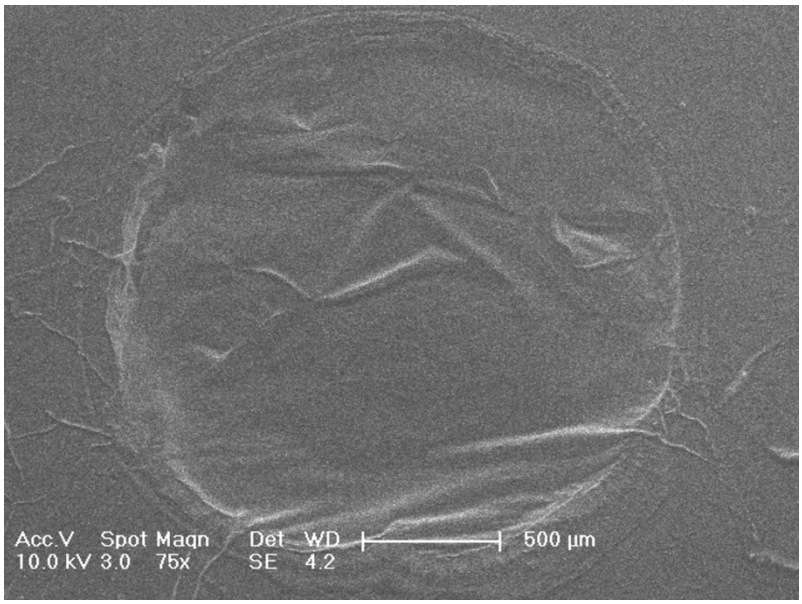

Figure 1. SEM image of the free-standing SWCNT film (2 mm diameter).

Figure 2

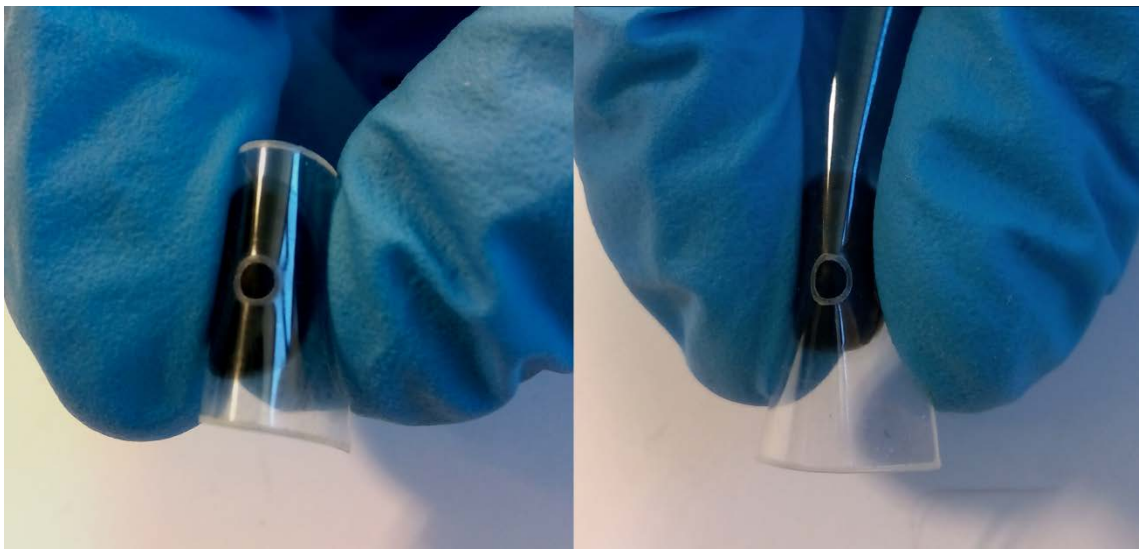

Figure 2. Free-standing SWCNT film bent in different directions.

Figure 3

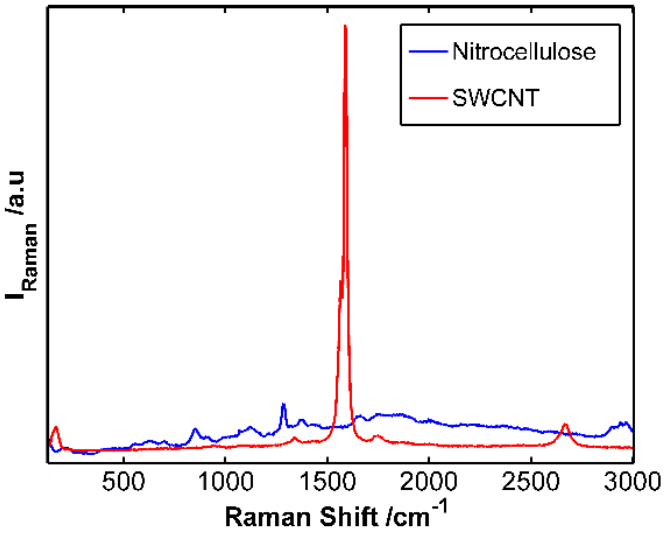

Figure 3. Raman spectra of the free-standing SWCNT film and the nitrocellulose filter.

Figure 4

(a)

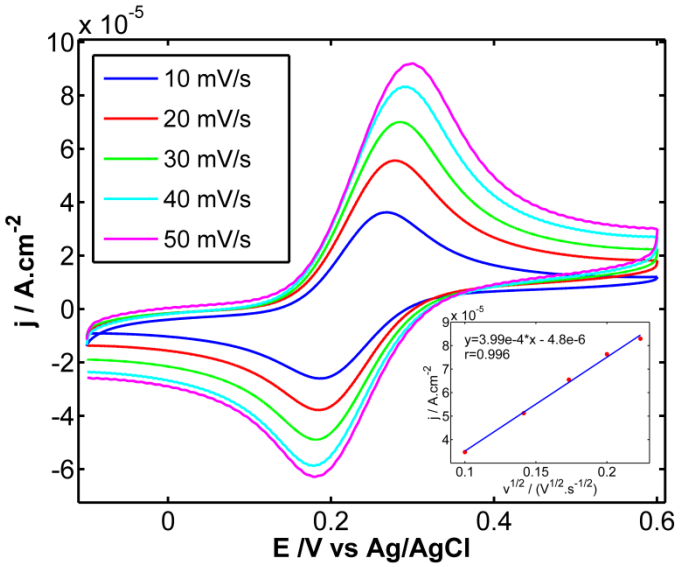

(b)

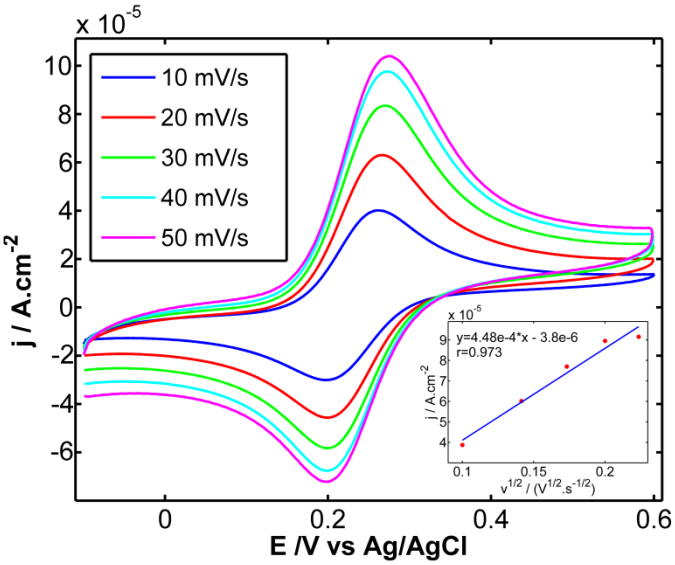

Figure 4. Cyclic voltammograms obtained in 5 × 10^{-4} M FcMeOH and 0.1 M KCl solution. The potential was scanned from -0.10 V to +0.60 V and back to -0.10 V at different scan rates. The same experiment was performed using (a) side A and (b) side B of the free-standing SWCNT film as working electrode. Insets: relationship between anodic peak current density and square root of scan rate.

Figure 5

(a)

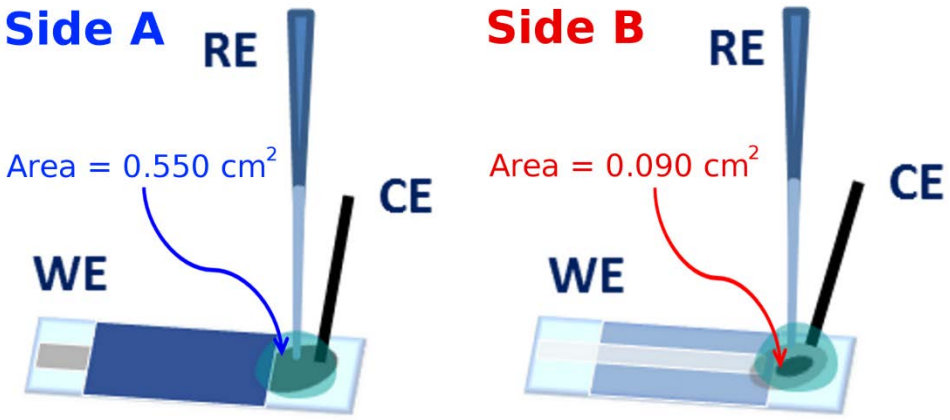

(b)

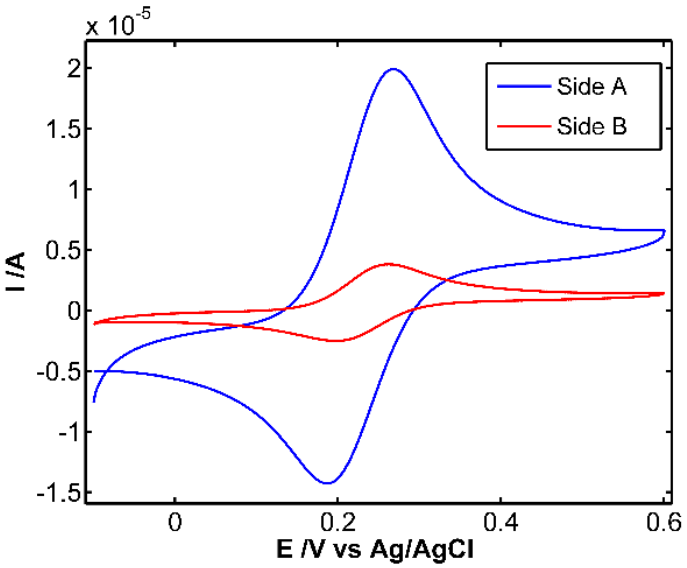

Figure 5. (a) Scheme of the electrochemical set-up when the different sides of the films are used. (b) Comparison between the current obtained during cyclic voltammetric experiments between -0.10 V to +0.60 V, at 0.01 V s^{-1}, in a 5 × 10^{-4} M FcMeOH and 0.1 M KCl solution using side A or side B as working electrode.

Figure 6

(a)

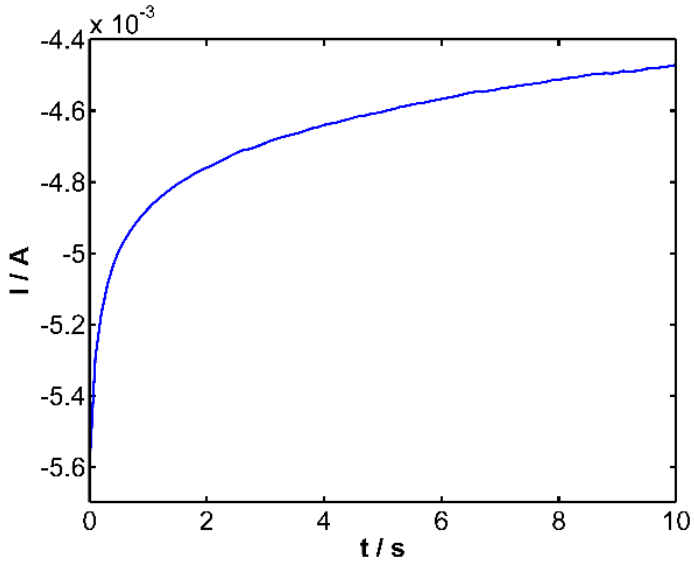
x 10^-3
-4.4
-4.6
-4.8
-5
-5.2
-5.4
-5.6
I / A
0
2
4
6
8
10
t / s

(b)

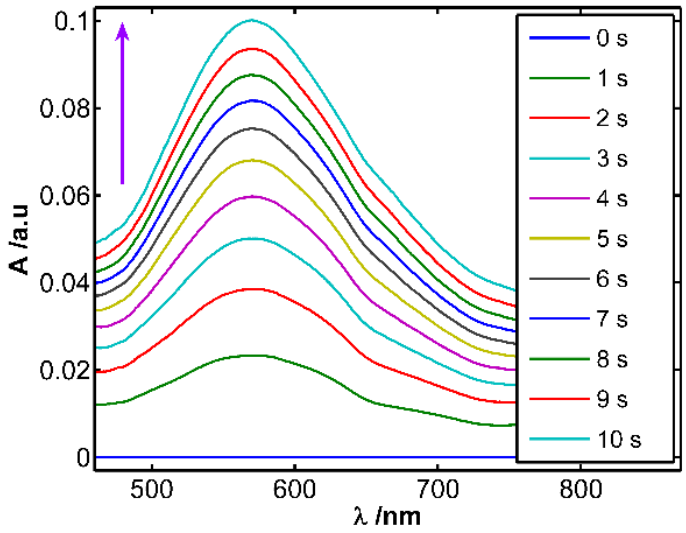
0.1
0.08
0.06
0.04
0.02
0
A /a.u
500
600
700
800
λ /nm
0 s
1 s
2 s
3 s
4 s
5 s
6 s
7 s
8 s
9 s
10 s

(c)

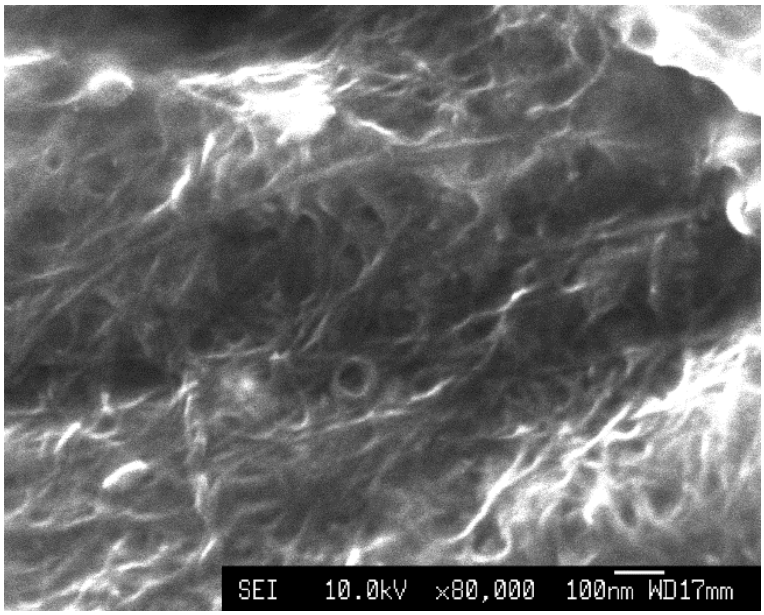

(d)

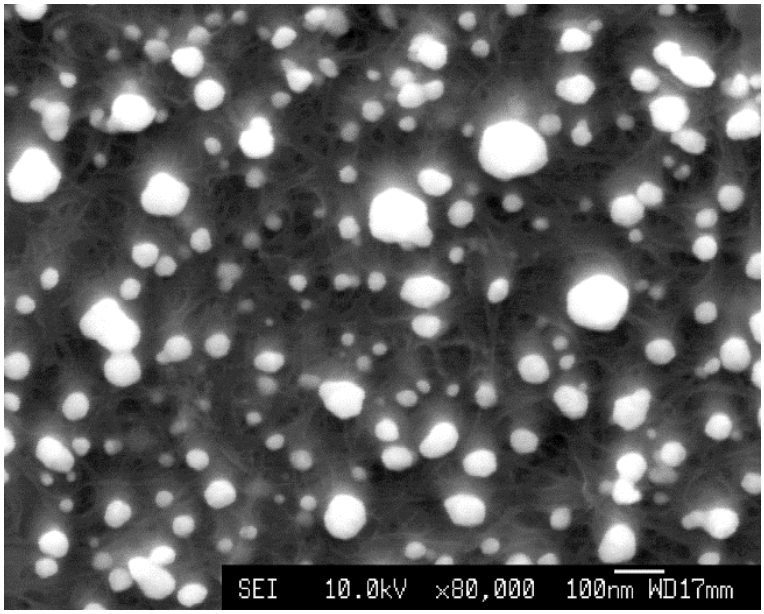

Figure 6. (a) Chronoamperometry response obtained during AuNPs electrodeposition applying -1.50 V for 10 s in 2.5×10^{-3} M $HAuCl_4$ and 0.1 M KCl. (b) UV-Vis spectra evolution with time, plotting one spectrum each second. SEM images of the film (c) before and (d) after the electrodeposition of AuNPs on side B of the free-standing SWCNT electrode.

Graphical abstract